Journal of Superconductivity and Novel Magnetism (2018) 31:2305–2312
https://doi.org/10.1007/s10948-017-4496-4

ORIGINAL PAPER

Synthesis of CdS Nanoparticles by Hydrothermal Method and Their Effects on the Electrical Properties of Bi-based Superconductors

N. Loudhaief[1] · H. Labiadh[1] · E. Hannachi[1] · M. Zouaoui[1] · M. Ben Salem[1]

Received: 24 August 2017 / Accepted: 28 November 2017 / Published online: 9 December 2017

Abstract
Cadmium sulfide (CdS) nanoparticles were synthesized by hydrothermal process and have been characterized by x-ray diffraction (XRD), transmission electron microscopy (TEM), and energy-dispersive x-ray spectroscopy (EDXS) system. The effect of added CdS nanoparticles on the superconducting properties and flux pinning capability in $(Bi,Pb)_2Sr_2Ca_2Cu_3O_y$ system (denoted as (Bi,Pb)-2223) has been reported. Hydrothermal method is an effective route to synthesize CdS nanoparticles with good crystallinity and having average grain size of about 12 nm. Then, small amounts (0–0.4 wt%) of nanosized CdS particles were added to Bi-2233 samples using a solid-state reaction route. The transport critical current densities and the electrical resistivity $\rho\,(T, H)$ were performed using the four-probe technique. The results show that samples sintered by small amount of CdS nanoparticles ($\leq$0.3 wt%) exhibit the higher critical current densities and energy pinning in applied magnetic fields compared to free added sample. Consequently, the addition of CdS could introduce effective pinning centers which account for the improvement in superconducting properties in the Bi-2223 materials.

Keywords Bi-2223 superconductors · Hydrothermal method · CdS nanoparticles · Superconducting properties · Flux pinning

1 Introduction

Semiconductor cadmium sulfide (CdS) nanoparticles have attracted considerable attention because of their wide direct band gap of 2.4 eV and their specific properties that are not observed by their bulk materials [1, 2]. Such nanoparticles are used in various fields such as optoelectronics, photonics, photovoltaics, and photocatalysis [2]. Based on previous studies, CdS nanostructures have been prepared using numerous physical and chemical techniques such as sol-gel [3], hydrothermal [1], solvothermal [4], co-precipitation [5], polyol [6], and microwave-assisted methods [7]. Among these different methods, low-temperature hydrothermal process is the most frequently used because of its non-toxicity, biocompatibility, eco-friendliness, and low-cost facility. Furthermore, by controlling various parameters such as temperature, reaction time, pressure, precursors, and surface ligands, one can get various dimensions, structure, and morphology of nanoparticles.

Since the discovery of Bi-based superconducting systems (BSCCO), several studies regarding the preparation methods, superconducting characteristics, and the structure of these compounds have been made [8–10]. Indeed, these materials have a particular place owing to their high critical transition temperature T_{co} and especially a good mechanical performance [11, 12]. Moreover, Bi-based superconducting materials are composed of the layered structures that make the mobile charge carriers confine to the $Cu–O_2$ layers [13, 14]. In the Bi-based superconducting compounds, there are three basic superconducting phases with respect to the number of $Cu–O_2$ planes in the unit cell. The phase which exhibits the high critical transition temperature $T_{co} = 110$ K corresponds to $Bi_2Sr_2Ca_2Cu_3O_{10}$ (denoted Bi-2233). Nevertheless, the main constraints of BSCCO superconductors are weak links between the grains resulting in weak critical current density J_c in bulk samples. The addition of

✉ M. Ben Salem
salemwiem2005@yahoo.fr

[1] Laboratory of Physics of Materials – Structure and Properties, Department of Physics, Faculty of Sciences of Bizerte, University of Carthage, 7021 Zarzouna, Tunisia

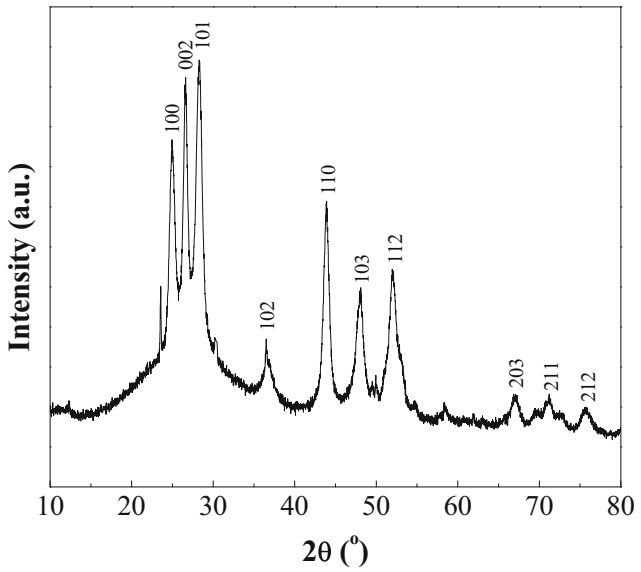

Fig. 1 X-ray powder diffraction patterns of CdS nanoparticles

nanosized particles or substitution of elements are one of the most effective ways for controlling the superconducting properties of high T_c superconductors (HTS) [15–21]. The improvement or devastation of the superconducting properties is heavily dependent on the characteristics of the dopant in the crystal structure. A suitable amount of nanometer particles can cause a significant improvement in the flux pinning ability and transport properties of compounds. Among various classes of nanoparticles, semiconductor nanoparticles have emerged as important materials with promising applications and have proved its effectiveness in improving the critical current densities in superconducting materials [22–24]. Although many papers have been already reported as regards to the effect of nanoparticles on the enhancement of the J_c, on the best of our knowledge, no report on the effect of CdS nanoparticles was published in the BSCCO system.

The first part of the present work concerns the synthesis of CdS nanoparticles via the hydrothermal method. Then, we have used the prepared nanoparticles as additives and we aim to study their effect on the superconducting properties and flux pinning mechanisms in BSCCO system.

2 Material and Methods

2.1 Nanoparticles Synthesis

Hydrothermal method was used to prepare semiconductor CdS nanoparticles starting from cadmium chloride hydrate

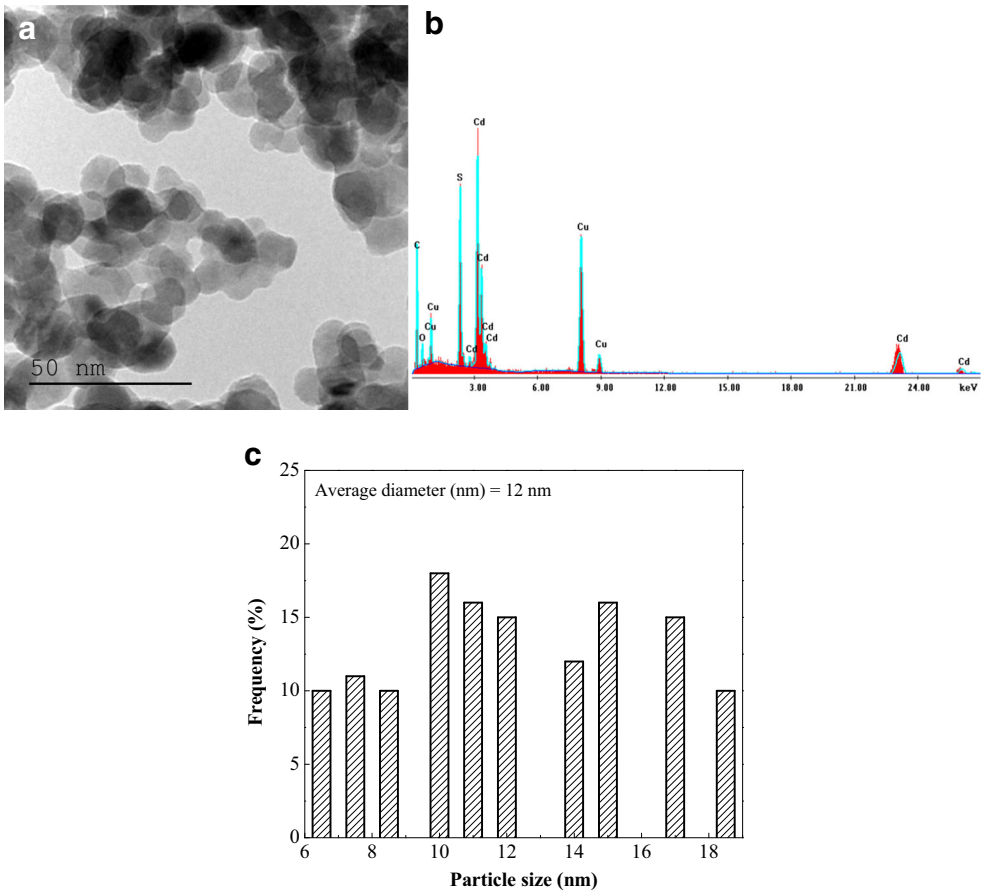

Fig. 2 **a** Transmission electron microscopy image of CdS nanoparticles prepared by hydrothermal method. **b** EDXS spectrum taken from the area with nanoscale entities. **c** The corresponding size distribution

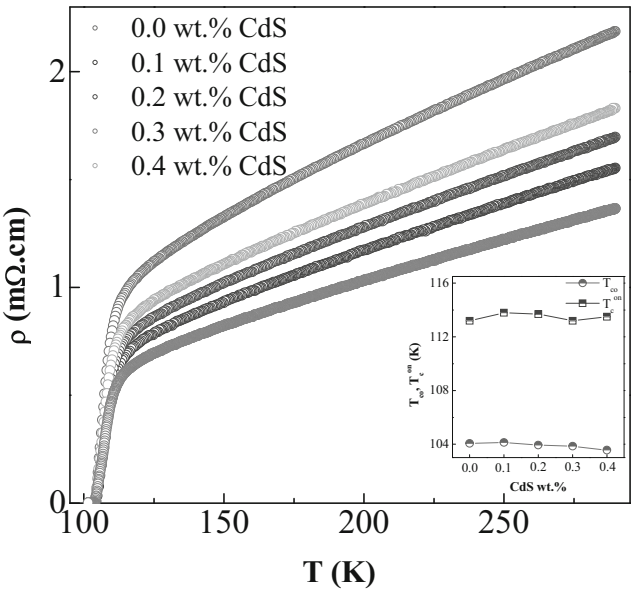

Fig. 3 Resistivity dependence on the temperature for samples added with various amounts of CdS nanoparticles. Inset: Evolutions of the zero-resistivity temperature T_{co} and the onset temperature of the superconducting transition T_c^{on} of samples sintered with different amounts of CdS

($CdCl_2$–H_2O) and thiourea CH_4N_2S as precursors and using propanoic acid $C_3H_6O_2$ as surface ligand, which is necessary in the stability of the nanocrystals. For the synthesis of CdS nanocrystals, 0.1006 g of $CdCl_2$–H_2O was dissolved in 5 ml of distilled water to obtain a 0.1-M solution, 0.0342 g of CH_4N_2S was dissolved in 4.5 ml of distilled water to obtain a 0.1-M solution, and 0.25 ml of propanoic acid was dissolved in 20 ml of distilled water. The cadmium chloride hydrate solution and propanoic acid solution were mixed together and then were dropped under vigorous stirring. To make a basic solution, a 2-M sodium hydroxide solution NaOH is added until a pH = 10. Thiourea solution is thereafter added to the previous solution as a source of sulfur. The result precursor mixture was stirred at room temperature for 24 h, placed into a teflon-lined autoclave, and finally subjected at heat treatment 180 °C for 7 h. The orange precipitates were collected, washed with ethanol for several times to remove soluble inorganic impurities, and then dried at 80 °C in air before further characterization. We have examined the structure, the average particle sizes, and the phase composition of the resulting product by powder XRD using a Philips 1710 diffractometer with CuK_α radiation and FEI Tecnai G2 transmission electron microscopy coupled with an energy-dispersive x-ray spectroscopy (EDXS) system. Figure 1 displays the XRD patterns of CdS nanoparticles. Strong and sharp diffraction peaks have been observed indicating the good crystallinity of the product. The indexed diffraction peaks in Fig. 1 correspond to the hexagonal

Table 1 Characteristic parameters of pure and CdS added samples

Samples	Characteristic parameters			
	T_c^{on}(K)	T_{co}(K)	ρ_o(mΩ cm)	$\alpha(\mu\Omega\, cm K^{-1})$
0.0 wt% CdS	113.20	104.07	0.45	6
0.1 wt% CdS	113.80	104.13	0.28	4.4
0.2 wt% CdS	113.70	103.94	0.32	4.8
0.3 wt% CdS	113.20	103.86	0.25	3.9
0.4 wt% CdS	113.50	103.57	0.35	5.1

structure with lattice parameters $a = 4.121$ Å and $c = 6.682$ Å. Figure 2a is a transmission electron microscopy image showing an almost monodispersion of nanoentities with oval or spherical shape. EDXS analyses performed on areas with nanosized particle indicate the presence of cadmium (Cd) and sulfur (S) elements (Fig. 2b). Based on statistical analysis of more than 100 entities in a single region (Fig. 2c), the average size of nanoparticles is about 12 nm. While the diameter of CdS nanoparticles, estimated with the Debyee-Scherrer formula, was found to be 10 nm, which is in good agreement with the TEM observations.

2.2 Superconducting Samples Preparation

Details of the preparation of BSCCO polycrystalline samples have been presented elsewhere [21] and we give herein a brief description. Samples were synthesized using solid-state reaction route by considering three thermal cycles comprising additives at the beginning of each cycle. During the final treatment phase, the synthesized CdS nanoparticles were added to BSCCO. The additional amount of CdS, varied from $x = 0$ to $x = 0.4$ wt% of the total mass of sample. The mixture were pressed into pellets under a uniaxial pressure of 1 GPa and finally sintered in air at 835 °C for 72 h. The temperature dependence of the electrical resistivity $\rho(T\,H)$ under applied magnetic fields ranging from 0 to 100 mT measurements and the current-voltage (I–V) characteristics were carried out using the four-probe technique. The critical current density (J_c) values were determined at various temperatures using a 5 μV/cm criterion. A magnetic field was applied along the short axis of the sample and the excitation current was injected along the length axis of the samples.

3 Results and Discussion

Measurements of the resistivity dependence on the temperature $\rho(T)$ for pure and CdS added Bi-2223 samples are shown in Fig. 3. All samples show (above the onset transition temperature (T_c^{on})) a metallic behavior in the

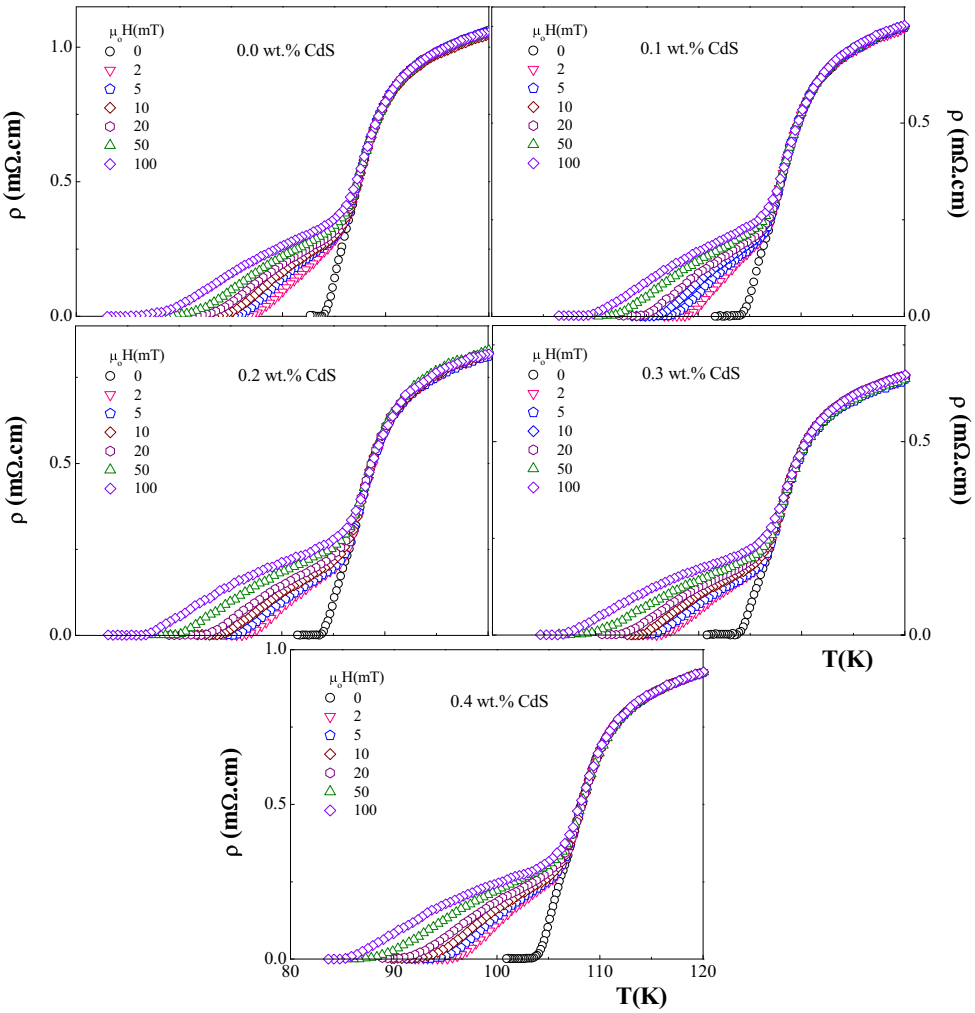

Fig. 4 Variations of the electrical resistivity with temperature at different applied magnetic fields of samples sintered with different amounts of CdS

normal state followed by a sharp superconducting transition to zero-resistivity T_{co} confirming the decrease of the porosity, grain boundary resistivity, and grain boundary weak links in the system. The resistivity curves in the metallic behavior can be expressed by the linear equation such as: $\rho_n(T) = \rho_o + \alpha T$, where ρ_o is an indicator of the sample homogeneity and defect density and the slope α is considered as a parameter that depends on the intrinsic electronic interaction. The obtained values of critical temperatures (T_c^{on}, T_{co}), ρ_o and α for pure and added samples are listed in Table 1. The data show that all CdS-added samples exhibit the lower normal-state resistivity and residual resistivity ρ_o. This implies the good quality process of synthesis and positive effect of CdS doping. Furthermore, it is clearly seen from the inset of Fig. 3 that the zeroresistance temperature, T_{co}, was practically maintained in Bi-2223 with different amounts of CdS. Also, we found an almost constant value of the onset temperature of the superconducting transition (T_c^{on} close to 114 K) for all sintered samples.

In order to examine the relevant effect of CdS addition under applied magnetic field (H), we have measured the resistivity of pure and CdS added samples with different values of magnetic fields. It is clearly seen from Fig. 4 that the lower region of the curves ($T < T_c$), where T_c is the peak temperature of the $\frac{d\rho}{dT}$ versus T curves, is strongly affected by the application of applied magnetic field. It is commonly known that the flow of superconducting carriers through the weak couplings and nanocrystallites is prevented by the application of a magnetic field. Indeed, an applied magnetic field is expected to suppress the critical

Table 2 Values of a and n obtained from $\rho(TH)$ measurements for free and CdS-added samples

Samples	0.0 wt% CdS	0.1 wt% CdS	0.2 wt% CdS	0.3 wt% CdS	0.4 wt% CdS
a	5.70	4.90	5.65	5.85	6.46
n	0.24	0.24	0.23	0.23	0.22

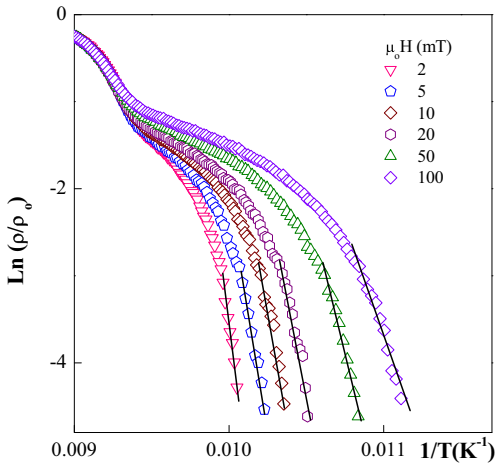

Fig. 5 Typical curve of $ln\frac{\rho}{\rho_o}$ versus $\frac{1}{T}$ at various magnetic fields

current of a Josephson junction and consequently result in the appearance of a junction resistance. We note that the addition of CdS nanoparticles narrows the width of the resistive transition width $\Delta T = T_{co}(0) - T_{co}(H)$. The ΔT data are well adjusted according to a scaling relationship of the power law $\Delta T = aH^{-n}$. In our case, the parameter n is found to be similar 0.23 ± 0.01 for all sintered samples. However, the values of the factor, a, are lower for samples sintered with CdS concentration <0.3 wt% as listed in Table 2. This result confirms the beneficial effect of CdS addition on the improvement of the electrical conduction in the material.

The dependence of $\rho(T, H)$ is expected to provide information about the mechanism of the vortices pinning. Indeed, the magneto-resistivity $\rho(T, H)$ curves in the polycrystalline HTSC has been found to obey to the Arrhenius relation as follows [25, 26]: $\rho(T, H) = \rho_o \exp\left(-\frac{U_o(T,H)}{k_B T}\right)$ where U_o is the flux pinning energy depends on both the temperature and the magnetic field and k_B is the Boltzmann constant. The U_o value can be directly

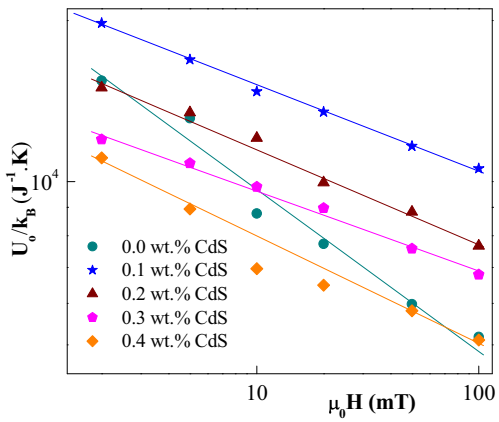

Fig. 6 Variations of the pinning energy U_o with applied magnetic fields for samples sintered with different amounts of CdS

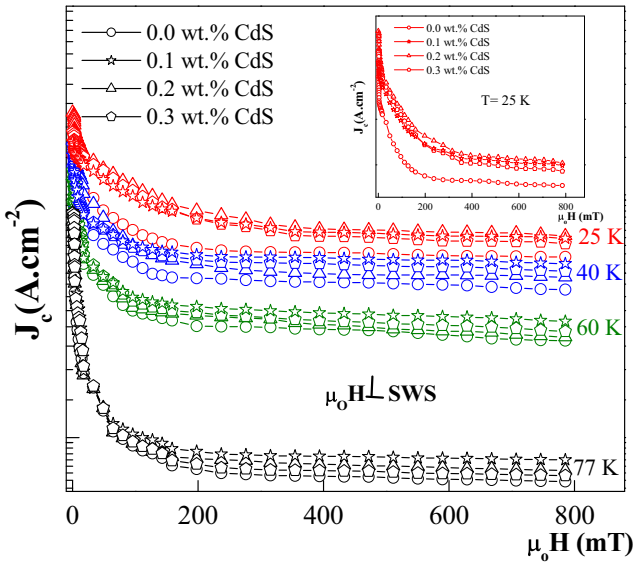

Fig. 7 The variation of the critical current density with applied magnetic fields of samples added with various amounts of CdS nanoparticles. Magnetic field was applied perpendicular to the samples wide surface

determined from the linear data in the tail part of the slope of the plot of $ln\frac{\rho}{\rho_o}$ versus $\frac{1}{T}$; a typical curve is depicted in Fig. 5. Figure 6 displays the deduced U_o, for different amounts of CdS addition. The value of U_o decreases as the magnetic field increases for each sample. Compared to CdS-added samples, the pure one shows a rapid decrease of U_o on magnetic field. Besides, it is clearly seen that U_o for samples sintered with CdS concentration <0.3 wt% is much higher than for a pure one in the whole range

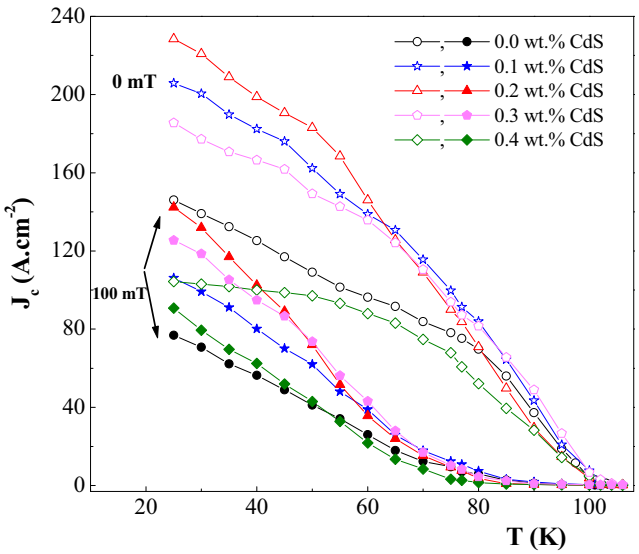

Fig. 8 Temperature dependence of critical current density in various applied magnetic fields for samples sintered with different amounts of CdS

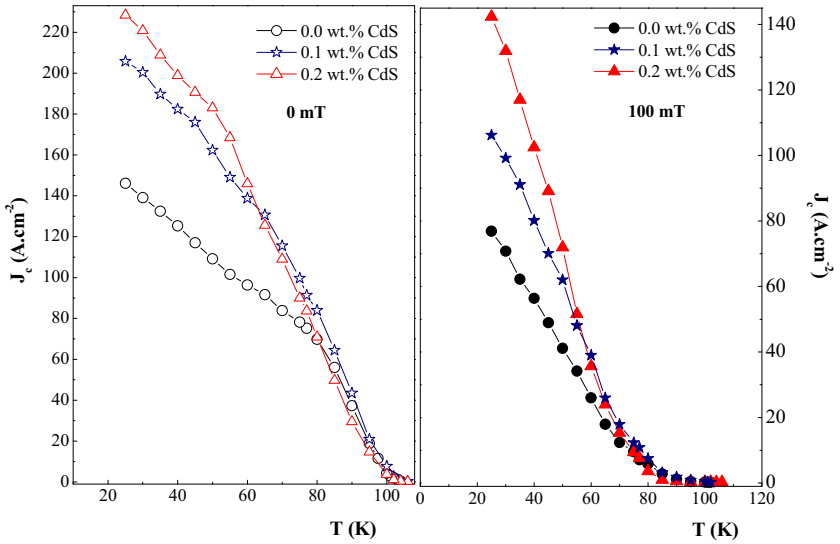

Fig. 9 Temperature dependence of critical current density at self and applied magnetic field for free and 0.1 and 0.2 wt% added samples

of the considered magnetic field. This result confirms the important role of CdS addition in improving the transport capabilities of Bi-2223 materials.

Figure 7 shows J_c measurements under applied magnetic fields. All sintered samples exhibit deterioration of J_c on increasing the magnitude of magnetic field. It is notable that J_c is increased for samples sintered with CdS throughout the whole range of applied magnetic fields. For lower temperatures, the CdS-added samples exhibit less sensitivity to magnetic fields compared with the non-added one (inset of Fig. 7). These results suggest that the CdS nanoparticles act as effective pinning centers yielding to the improvement of critical current density behavior.

Figure 8 shows the temperature dependences of critical current densities at applied magnetic field for free and CdS-added samples. The critical current density increase monotonically on decreasing temperature from near T_{co} down to $T = 25$ K for each sample. The samples sintered with CdS concentration $\leq$0.3 wt% exhibit the highest values of J_c in almost the entire temperature range at self-magnetic

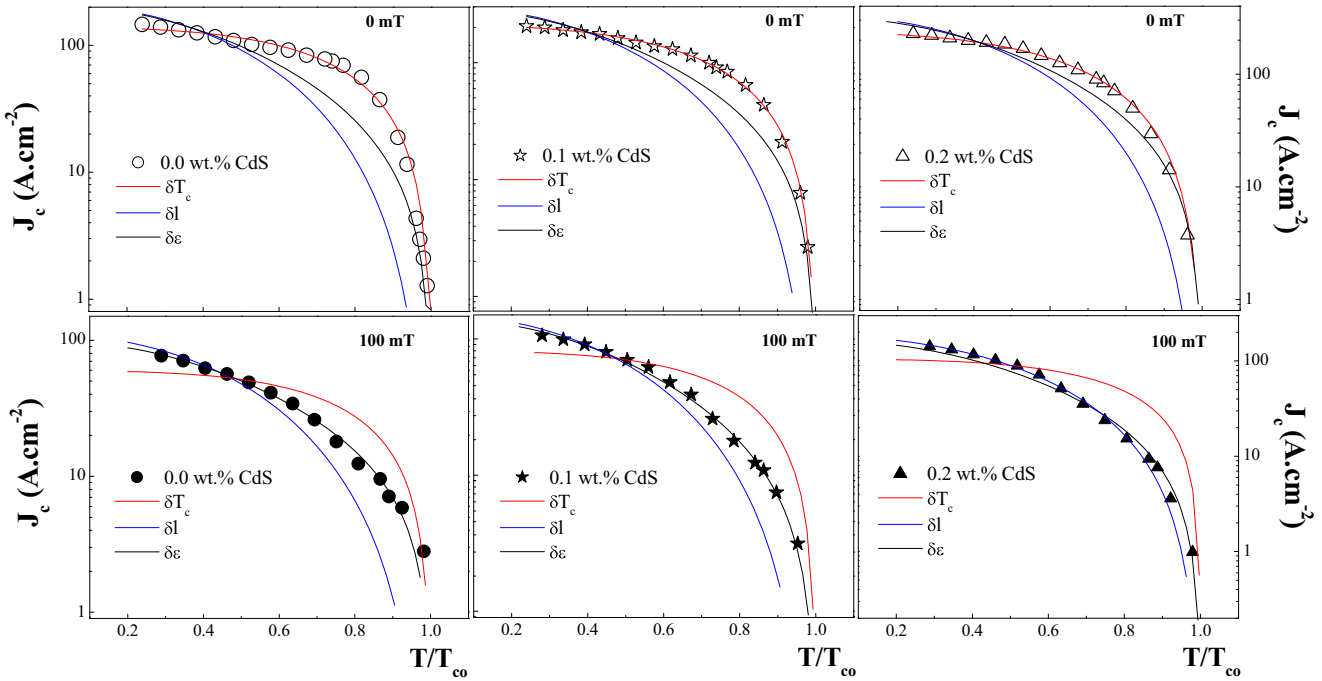

Fig. 10 Temperature dependence of the current density J_c at magnetic fields of 0 and 100 mT for free and 0.1 and 0.2 wt% added samples. Scatters mark the experimental data. Lines are theoretical fits obtained based on the model of the δl (blue curves), the δT_c (red curves), and the $\delta \varepsilon$ (black curves) pinning mechanisms

field; however, when the addition of CdS exceeds 0.4 wt%, one can observe a decrease of $J_c(T)$ values. For an applied magnetic field (i.e., 100 mT), we note that the values of $J_c(T)$ remain very higher for samples sintered with a small amounts of CdS ($\leq$0.3 wt%) compared to the non-added one. For clarity, we have plotted in Fig. 9 the temperature dependence $J_c(T)$ for 0.0, 0.1, and 0.2 wt% CdS-added samples. A comparison between samples shows that the critical current density of the added samples has increased for the whole-temperature range either on self or applied magnetic field. This effect could be the result of further homogeneity and better connection between the superconducting grains following the addition of CdS. Therefore, it seems that small amount of CdS nanoparticles are acting as conductors. So, it can enhance the connections of grains boundary of BSCCO compound and improve the transport the electrical current in the material.

In order to determine the contribution of each pinning mechanism for free and CdS-added samples, we have analyzed the critical current density dependences on temperature $J_c(T)$ based on the thermally activated flux motion and the collective flux-pinning models [27]. For HTS materials, the pinning mechanism can be classified into three types: (1) δT_c, which is due to the randomly distributed spatial variations in the transition temperature T_c [28]; (2) δl, mostly due to crystal lattice defects and related to spatial fluctuation of the charge-carrier mean free path [27]; and (3) $\delta\varepsilon$, due to the stress/strain field [29]. According to these models, the global transport critical current density $J_c(T)$ is expressed as follows:

$$J_c(T) \approx J_c(0)\,(1-t^2)^{\alpha}(1+t^2)^{\beta} \tag{1}$$

where $J_c(0)$ is the critical current density at 0 K, $t = \frac{T}{T_{co}}$ is the reduced temperature, and the exponents α and β are related to the pinning mechanism;

$$\text{for the } \delta\varepsilon \text{ pinning mechanism, } J_c(T) = J_c(0)\,(1-t^2)^{\frac{7}{6}}(1+t^2)^{-\frac{11}{6}} \tag{2}$$

$$\text{for } \delta T_c \text{ pinning mechanism, } J_c(T) = J_c(0)\,(1-t^2)^{\frac{7}{6}}(1+t^2)^{\frac{5}{6}} \tag{3}$$

$$\text{and for } \delta l \text{ pinning mechanism, } J_c(T) = J_c(0)\,(1-t^2)^{\frac{5}{2}}(1+t^2)^{-\frac{1}{2}} \tag{4}$$

Figure 10 shows the plots of the experimental data $J_c(T)$ for free, 0.1 and 0.2 wt% CdS-added samples. The theoretical curves of (2), (3), and (4) are also presented in the figure by the solid lines. As can be seen, the experimental $J_c(T)$ values at self-applied magnetic fields are in a good agreement with the model of δT_c pinning over the main temperature range for all sintered samples. However, for an applied magnetic field $\mu_o H = 100$ mT, the δT_c pinning mechanism suppressed completely and $J_c(T)$ values agree with the $\delta\varepsilon$ mechanism for pure sample while the experimental results of CdS added samples cannot be explained by a single model over the whole region of the $J_c(T)$ curves. Indeed, the δl pinning mechanism is mainly responsible at low temperatures, decreased with increasing temperature, and then transformed to $\delta\varepsilon$ at temperatures close to T_{co}. It can be noted that the addition of CdS nanoparticles inside the superconducting matrix causes the fluctuations in the mean free path that are responsible for the δl pinning at low temperatures. Similar behavior has been found in the case of nano-Si-doped MgB_2 superconductor [30]. These results provide strong evidence that the CdS nanoparticles produced very strong pinning centers in the Bi-2223 matrix.

4 Conclusion

CdS nanoparticles with average grain size of about 12 nm were successfully synthesized by hydrothermal method. The effect of nanosized CdS particles addition on the superconducting properties of polycrystalline Bi-2223 compounds was systematically studied. CdS nanoparticles were added up to 0.4 wt% to Bi-2223 superconductors using solid-state reaction. The results of $\rho(T)$ measurements show that the addition of CdS has acted in an effective manner and decreased the normal-state resistivity and the residual resistivity ρ_o. It also showed that the onset temperature of the superconducting transition, T_c^{on}, and the zero-resistance temperature, T_{co}, values were maintained in Bi-2223 bulks with the addition of CdS nanoparticles. From the measurement of $\rho(TH)$, we have found that samples sintered by small amount of CdS possess a narrower resistive transition width ΔT under applied magnetic fields and higher values of pinning energy indicating the beneficial role of CdS nanoparticles on the improvement of the electrical conduction in the material. Critical current densities J_c were also investigated under applied magnetic fields at various temperatures. It is revealed that Bi-2223 bulk sintered with low concentration of CdS exhibits higher J_c values under applied magnetic fields compared to the pure one. From the temperature dependence of the critical currents, we have evaluated the pinning mechanism. The results show that the addition of CdS nanoparticles favors more than one pinning mechanism. It therefore concluded that the CdS nanoparticles produced very strong pinning centers in the Bi-2223 matrix. So an enhancement can be beneficial in J_c of CdS-added Bi-2223 compounds for the practical applications of these high temperature superconducting materials.

References

1. Chen, R., Han, B., Yang, L., Yang, Y., Xu, Y., Mai, Y.: Controllable synthesis and characterization of CdS quantum dots by a microemulsion-mediated hydrothermal method. J. Lumin. **172**, 197–200 (2016)
2. Qutub, N., Sabir, S.: Optical, thermal and structural properties of CdS quantum dots synthesized by a simple chemical route. Int. J. Nanosci. Nanotechnol. **8**, 111–120 (2012)
3. Zhang, H.: Effects of post-annealing treatment on the structure and photoluminescence properties of CdS/PS nanocomposites prepared by sol-gel method. Optoelectron. Lett. **12**, 81–84 (2016)
4. Ren, B., Cao, M., Zhang, Q., Huang, J., Zhao, Z., Jin, X., Li, C., Shen, Y., Wang, L.: Controllable synthesis of CdS nanowire by a facile solvothermal method and its temperature dependent photoluminescent property. J. Alloys Compd. **659**, 74–81 (2016)
5. Elavarthi, P., Kumar, A.A., Murali, G., Reddy, D.A., Gunasekhar, K.R.: Room temperature ferromagnetism and white light emissive CdS:Cr nanoparticles synthesized by chemical co-precipitation method. J. Alloys Compd. **656**, 510–517 (2016)
6. Darwish, M., Mohammadi, A., Assi, N.: Microwave-assisted polyol synthesis and characterization of pvp-capped CdS nanoparticles for the photocatalytic degradation of tartrazine. Mater. Res. Bull. **74**, 387–396 (2016)
7. Yang, H., Huang, C., Li, X., Shi, R., Zhang, K.: Luminescent and photocatalytic properties of cadmium sulfide nanoparticles synthesized via microwave irradiation. Mater. Chem. Phys. **90**, 155–158 (2005)
8. Maeda, H., Tanaka, Y., Fukutomi, M., Asano, T.: A new high-T_c oxide superconductor without a rare earth element. Jpn. J. Appl. Phys. **27**, L209 (1988)
9. Ozturk, O., Yegen, D., Yilmazlar, M., Varilci, A., Terzioglu, C.: The effect of cooling rates on properties of $Bi_{1.7}Pb_{0.35}Sr_{1.9}Ca_{2.1}Cu_3O_y$ superconductors produced by solid-state reaction method. Physica C **451**, 113–117 (2007)
10. Michel, C., Hervieu, M., Borel, M.M., Grandin, A., Deslandes, F., Provost, J., Raveau, B.: Superconductivity in the Bi-Sr-Cu-O system. Z. Phys. B: Condens. Matter **68**, 421–423 (1987)
11. Yildirim, G., Varilci, A., Akdogan, M., Terzioglu, C.: Role of annealing time and temperature on structural and superconducting properties of (Bi, Pb)-2223 thin films produced by sputtering. J. Mater. Sci: Mater. Electron. **23**, 928–935 (2012)
12. Sarkar, K.A., Maartense, I., Peterson, T.L., Kumar, B.: Preparation and characterization of superconducting phases in the Bi(Pb)SrCaCuO system. J. Appl. Phys. **66**, 3717–3722 (1989)
13. Zhang, H., Sato, H.: Universal relationship between T_c and the hole content in p-type cuprate superconductors. Phys. Rev. Lett. **70**, 1697–1699 (1993)
14. Ghahfarokhi, S.E.M., Shoushtari, M.Z.: Structural and physical properties of Cd-doped $Bi_{1.64}Pb_{0.36}Sr_2Ca_{2-x}Cd_xCu_3O_y$ superconductor. Physica B **405**, 4643–4649 (2010)
15. Halim, S.A., Khawaldeh, S.A., Mohamed, S.B., Azhan, H.: Superconducting properties of $Bi_{2-x}Pb_xSr_2Ca_2Cu_3O_y$ system derived via sol-gel and solid state routes. Mater. Chem. Phys. **61**, 251–259 (1999)
16. Dos Santos, C.A.M., Moehlecke, S., Kopelevich, Y., Machado, A.J.S.: Inhomogeneous superconductivity in $Bi_2Sr_2Ca_{1-x}Pr_xCu_2O_{8+\delta}$. Physica C **390**, 21–26 (2003)
17. Biju, A., Abhilash Kumar, R.G., Aloysius, R.P., Syamaprasad, U.: Structural and superconducting properties of $Bi_{1.7}Pb_{0.4}Sr_{2-x}Gd_xCa_{1.1}Cu_{2.1}O_y$ system. Physica C **449**, 109–115 (2006)
18. Awana, V.P.S., Agarwal, S.K., Narlikar, A.V., Das, M.P.: Superconductivity in Pr- and Ce-doped $Bi_2CaSr_2Cu_2O_y$ systems. Phys. Rev. B **48**, 1211–1216 (1993)
19. Berger, H., Ariosa, D., Gaal, R., Saleh, A., Margaritondo, G., Lee, S.F., Huang, S.H., Chang, H.W., Chuang, T.M., Liou, Y., Yao, Y.D., Hwu, Y., Je, J.H., Gasparov, L.V., Tanner, D.B.: Coexistence of ferromagnetism and high-temperature superconductivity in Dy-Doped BiPbSrCaCuO. Surf. Rev. Lett. **9**, 1109–1112 (2002)
20. Ghattas, A., Annabi, M., Zouaoui, M., Ben Azzouz, F., Ben Salem, M.: Flux pinning by Al-based nano particles embedded in polycrystalline (Bi,Pb)-2223 superconductors. Physica C **468**, 31–38 (2008)
21. Zouaoui, M., Ghattas, A., Annabi, M., Ben Azzouz, F., Ben Salem, M.: Effect of nano-size ZrO_2 addition on the flux pinning properties of (Bi, Pb)-2223 superconductor. Supercond. Sci. Technol. **21**, 125005 (2008)
22. Ben Salem, M.K., Hannachi, E., Slimani, Y., Hamrita, A., Zouaoui, M., Bessais, L., Ben Salem, M., Ben Azzouz, F.: SiO_2 nanoparticles addition effect on microstructure and pinning properties in $YBa_2Cu_3O_y$. Ceram. Int. **40**, 4953–4962 (2014)
23. Guo, Y.C., Tanaka, Y., Kuroda, T., Dou, S.X., Yang, Z.Q.: Addition of nanometer SiC in the silver-sheathed Bi2223 superconducting tapes. Physica C **311**, 65–74 (1999)
24. Ben Salem, M.K., Almessiere, M.A., Al-Otaibi, A.L., Ben Salem, M., Ben Azzouz, F.: Effect of SiO_2 nano-particles and nano-wires on microstructure and pinning properties of $YBa_2Cu_3O_{7-d}$. J. Alloys Compd. **657**, 286–295 (2016)
25. Kim, J.J., Lee, H., Chung, J., Shin, H.J., Lee, H.J., Ku, J.K.: Flux-creep dissipation in epitaxial $YBa_2Cu_3O_{7-\delta}$ film: Magnetic-field and electrical-current dependence. Phys. Rev. B **43**, 2962–2967 (1991)
26. Koch, R.H., Foglietti, V., Gallagher, W.J., Koren, G., Gupta, A., Fisher, M.P.A.: Experimental evidence for vortex-glass superconductivity in Y-Ba-Cu-O. Phys. Rev. Lett. **63**, 1511–1514 (1989)
27. Blatter, G., Feigel'man, M.V., Geshkenbein, V.B., Larkin, A.I., Vinokur, V.M.: Vortices in high-temperature superconductors. Rev. Mod. Phys. **66**, 1125–1388 (1994)
28. Wen, H.H., Zhao, Z.X., Xiao, Y.G., Yin, B., Li, J.W.: Evidence for flux pinning induced by spatial fluctuation of transition temperatures in single domain $(Y_{1-x}Pr_x)Ba_2Cu_3O_{7-\delta}$ samples. Physica C **251**, 371–378 (1995)
29. Wen, H.H., Zhao, Z.X., Wang, R.L., Li, H.C., Yin, B.: Evidence for the lattice-mismatch-stress-field induced flux pinning in $(Gd_{1-x}Y_x)Ba_2Cu_3O_{7-\delta}$ thin films. Physica C **262**, 81–88 (1996)
30. Ghorbani, S.R., Wang, X.L., Hossain, M.S.A., Dou, S.X., Lee, S.I.: Coexistence of the δl and δT_c flux pinning mechanisms in nano-Si-doped MgB_2. Supercond. Sci. Technol. **23**, 025019 (2010)